·Clinical Research·

Characterization of human retinal vessel arborisation in normal and amblyopic eyes using multifractal analysis

Ştefan Tălu[1], Cristina Vlădutiu[2], Carmen A. Lupaşcu[3]

[1]Discipline of Descriptive Geometry and Engineering Graphics, Department of Automotive Engineering and Transportation, Faculty of Mechanical Engineering, Technical University of Cluj-Napoca, Cluj-Napoca 400641, Cluj, Romania

[2]Discipline of Ophthalmology, Department of Surgical Specialties and Medical Imaging, Faculty of Medicine, "Iuliu Hatieganu" University of Medicine and Pharmacy Cluj-Napoca, Cluj-Napoca 400012, Cluj, Romania

[3]Department of Mathematics and Informatics, University of Palermo, Palermo 90123, Italy

Correspondence to: Ştefan Tălu. Discipline of Descriptive Geometry and Engineering Graphics, Department of Automotive Engineering and Transportation, Faculty of Mechanical Engineering, Technical University of Cluj-Napoca, Cluj-Napoca 400641, Cluj, Romania. stefan_ta@yahoo.com

Received: 2014-06-12 Accepted: 2014-08-22

Abstract

• AIM: To characterize the human retinal vessel arborisation in normal and amblyopic eyes using multifractal geometry and lacunarity parameters.

• METHODS: Multifractal analysis using a box counting algorithm was carried out for a set of 12 segmented and skeletonized human retinal images, corresponding to both normal (6 images) and amblyopia states of the retina (6 images).

• RESULTS: It was found that the microvascular geometry of the human retina network represents geometrical multifractals, characterized through subsets of regions having different scaling properties that are not evident in the fractal analysis. Multifractal analysis of the amblyopia images (segmented and skeletonized versions) show a higher average of the generalized dimensions (D_q) for q=0, 1, 2 indicating a higher degree of the tree-dimensional complexity associated with the human retinal microvasculature network whereas images of healthy subjects show a lower value of generalized dimensions indicating normal complexity of biostructure. On the other hand, the lacunarity analysis of the amblyopia images (segmented and skeletonized versions) show a lower average of the lacunarity parameter Λ than the corresponding values for normal images (segmented and skeletonized versions).

• CONCLUSION: The multifractal and lacunarity analysis may be used as a non –invasive predictive complementary tool to distinguish amblyopic subjects from healthy subjects and hence this technique could be used for an early diagnosis of patients with amblyopia.

• KEYWORDS: retina; retinal vessels; amblyopia; strabismus; multifractals; lacunarity

DOI:10.3980/j.issn.2222-3959.2015.05.26

Tălu S, Vlădutiu C, Lupaşcu CA. Characterization of human retinal vessel arborisation in normal and amblyopic eyes using multifractal analysis. *Int J Ophthalmol* 2015;8(5):996-1002

INTRODUCTION

Amblyopia, often referred to by the public as "lazy eye", is a common developmental disorder of vision affecting approximately 1%-3% of the general population being the leading cause of decreased vision among children. Amblyopia is caused by abnormal visual stimulation during visual development, resulting in abnormalities in the visual centers of the brain. Functional amblyopia only develops in children between birth and 6-8y, although it may persist for life once established[1].

Amblyopia is clinically defined as decreased visual acuity in an otherwise healthy and properly corrected eye (acuities most frequently range from 20/30 to 20/60). Reduced visual acuity in the affected eye usually coexists with normal acuity in the patient's other eye[2].

In amblyopia there are two major etiologies: 1) unequal interocular refractive error or 2) a deviated eye. If the early impairment is unbalanced refractive error, the amblyopia is termed anisometropic, whereas amblyopia secondary to ocular deviation is termed strabismic. In some cases, both anisometropia and strabismus can be present concurrently[2].

The relationship between strabismus, anisometropia, and amblyopia is complex, and the conditions associated with amblyopia in adulthood may not be the ones that were important in creating amblyopia [3]. Amblyopia might be multifactorial, but it could also be a simpler abnormality that varies in severity but not in kind[3].

Classification of amblyopia is based on clinical conditions responsible for its development and can be used as a practical method to identify its etiology and apply a better management strategies.

The space-filling properties of complex branching biological structures can be characterized using morphological, topological and geometrical continuous-space concepts[4].

The three-dimensional human retinal microvascular network, as a complex structure, can be observed directly and non-invasively in its natural living state using a retinal camera[5-9].

To describe the morphology of human retinal vessel networks in fundus eye images, different methods are used in modern ophthalmology based on the measurement of tortuosity[10,11], width[10], branching angle[10], branching coefficient[10], fractal dimension[9-11] and of multifractal spectra[11,12].

Retinal microvascular abnormalities have been associated with vascular and non-vascular pathology as: diabetic macular edema[12]; dementia, cognitive functioning, and brain imaging abnormalities, including atrophy and vascular lesions[13]; diabetes and retinopathy[14]; chronic kidney disease and microalbuminuria[15]; and coronary artery diseases[16].

The human retinal vascular network has a branching pattern and it is considered to be a fractal structure at low resolution, in a "scaling window" which normally ranges in two to three orders of magnitude [11,17].

Images representing morphologically complex structures of the retinal vessel branching can be characterised by means of the fractal geometry[18-22].

The fractal dimension D of retinal vascular network quantifies the global measure of complexity of the vascular branching pattern [9,20]. Because the 3-dimensional retinal microvascular network structure is a geometric projection into a digital retinal image from the 2-dimensional space, its fractal dimension should be greater than 1 but less than 2.

In various fractal analysis studies, the average values of the estimated fractal dimensions that characterise the branching pattern of normal human retinal vessels were approximately 1.7 [9,18,19,21]. Generally, arterioles have a lower fractal dimension than venules [23]. However, in all of these studies for digital retinal images different methods of calculation of the fractal dimension have been used under various experimental conditions, different digital fundus cameras, different fields of view, using red-free fundus photographs, as well as fluorescein angiograms[9,18-22,24-26].

Some investigators observed a significant decrease in the fractal dimensions of human retinal vascular network with aging, consistent with observations from other human organ systems [20]. In different studies, investigators have found various values of the fractal dimensions associated with the retinal pathological status[24-26].

In various fractal analysis studies [9,12,22,26], investigators have applied the lacunarity analysis as a complementary multiscale method to characterize the branching pattern of retinal vessel networks that are inherent in high resolution retinal imagery and to specify an optimal spatial extent for spatial image information extraction. Its capability to detect multiple pattern scales and to discriminate between different types of heterogeneity was helpful in high resolution retinal imagery[9,12,22,26]. On the other hand, this method allows readily interpretable graphic representations and can be easily implemented[9,12,22].

Another method to characterize the branching pattern of retinal vessel networks is the multifractal approach that requires an infinite number of indices to characterize their scaling properties[9,12,26-28].

Multifractal analysis, as a useful tool for the study of non-uniform distributions, reveals more information about geometrical features and spatial distribution (a description over the retinal regions both locally and globally) and is far more sensitive in detecting small changes of the retinal microvasculature than the fractal analysis (a globally description over the retinal regions)[12, 26, 27].

In a recent study [27] using a multifractal methodology, the generalized fractal dimensions with average ±standard deviation (D_q for q=0, q=1 and q=2; where q is a real parameter that indicates the order of the moment of the measure) were estimated for normal retinal blood vessels using the box-counting method with next values: the capacity (or box-counting) dimension, D_0 =1.6968 ±0.0014; the information (Shannon entropy) dimension, D_1 =1.6246 ± 0.0011 and the correlation dimension, D_2=1.5921 ±0.0008. All generalized fractal dimensions being different and satisfying the relation: $D_0 > D_1 > D_2$ [27].

However, researchers have not reached a general consensus concerning the correlations between generalized fractal dimensions and pathological retinal diseases[12,26,28].

Despite recent studies in describing the organizational complexity and interactivity of the retinal microvasculature network, much remains to be learned.

The fractal and multifractal analysis of human retinal vascular network depends on the fractal methods, including the algorithm and specific calculation used *etc.*[21,29-32].

Different investigators have established that the fractal dimensions of fundus eye images corresponding to the strabismus states of the retina have higher average values in comparison with the corresponding values of the normal cases[22,24].

To our knowledge, this is the first multifractal analysis study of retinal microvascular network in amblyopic eyes in the available ophthalmologic literature.

SUBJECTS AND METHODS

Multifractal Analysis The multifractal theory concepts with the entire multifractal algorithm applied in this study (based on a practical method defined by Chhabra and Jensen [33]) has been previously described in detail by Tălu[11].

For a profile's binary image defined by a number of pixels, and covered by individual boxes, the probability (P_i) of finding them in a given box, which constitutes the measure of the analyzed set, is given by next formula[34].

$$P_i(r) = L_i(r)/L_T(r) \quad (1)$$

where: r-box size in the given scale; L_i -number of pixels in one box in the given scale r; L_T-total number of pixels in all boxes in the given scale r. High values of the selective parameter $q$enhance cells with relatively high values for P_i ; while low values of q favor cells with relatively low values of P_i [34].

In this study, by applying the multifractal analysis methods are determined the functional dependences D_q versus q and $f(\alpha)$ versus α; where the plot $f(\alpha)$ is called a multifractal spectrum, which presents the whole spectrum of fractal dimensions and $\alpha(q)$ represents Hölder exponents of the qth order moment. For $q=\pm\infty$, $\alpha_{min}=D_{-\infty}$ and $\alpha_{max}=D_{\infty}$. The singularity spectrum α-$f(\alpha)$ quantitatively describes the relationship of the singularity strength α and Hausdorff dimension with the multifractal measure[35]. Also, the plots of $f(\alpha)$ versus q and of $\alpha(q)$ versus q provide additional equivalent descriptions in multifractal analysis. The plot $\tau(q)$ (the mass correlation exponent of the qth order) also could be considered as a characteristic function of the multifractal behavior[36].

Lacunarity Analysis Lacunarity as a complementary multiscale method to interpret the scale-dependent measure of the heterogeneity or texture of the fractal object, can distinguish between fractal objects with the same fractal dimension[29,37].

The lacunarity concept [29,37] and lacunarity estimation method applied in this study (based on a mathematical algorithm implemented in the FracLac V 2.5[38] for ImageJ software) has been previously described in detail by Tălu[12].

Lacunarity explicitly characterize the spatial organization of an image, and its composing sub-units and can be used with both binary and quantitative data in one, two, and three dimensions [22,39]. Lacunarity measures the distribution of gap sizes: low lacunarity geometric objects are homogeneous because all gap sizes are the same, whereas high lacunarity objects are heterogeneous [39]. High lacunarity values are associated with the presence of large gaps or holes; while a fractal that is translationally invariant has characteristically low lacunarity[39].

In this study, lacunarity (λ) was determined as the variation in pixel density for an image, computed from scans at different box sizes and different grid orientations [38,39]. The mean $\overline{\lambda}$ (or Λ) was expressed as[38]:

$$\Lambda = \frac{1}{n}\left(\sum_{j=1}^{g}\sum_{i=1}^{n}\left[1+(\sigma/\mu)^2\right]\right) \quad (2)$$

where: σ is the standard deviation of the number of pixels that were in a box of size; μ is the mean for pixels per box at this size, ε is in a box count at this orientation, g and n is the number of box sizes.

Segmentation Method The choice of vessel segmentation method is based on the diagnostic application, morphologic parameters to be evaluated, accuracy requirement, and tolerance to imaging defects[10]. In our study, the segmentation of retinal vessels images was made using an automatic unsupervised method [40-42]. The unsupervised segmentation method with the entire multifractal algorithm applied in this study has been previously described in detail by Lupaşcu *et al* [40-42]. Finally, a post-processing fills pixel gaps in detected blood vessels and removes falsely-detected isolated vessel pixels.

Multifractal and Lacunarity Analysis The clinical protocol was reviewed and approved by the local Ethics Committee of the "Iuliu Hatieganu" University of Medicine and Pharmacy, Cluj-Napoca, Romania and was adhered to the tenets of the Declaration of Helsinki for research in human subjects. The written informed consent was obtained from the child's parents.

A set of 12 human digital retinal images, corresponding to both normal (6 images) and amblyopia states of the retina (6 images), from amblyopic children treated in the Ophthalmological Clinic in Cluj-Napoca, Romania, between January 2012 and December 2013, was selected for analysis.

Six patients (50%) were female and six (50%) male. Each subject underwent a full ophthalmic examination. The control group have the same examinations with the pathological group. The inclusion criteria of the healthy controls included the following: 1) no symptoms or signs of amblyopia; 2) no amblyopia history; 3) no amblyopia family history; 4) no ocular disease.

The slides were captured by a fundus camera at 45° field of view (VISUCAM^{Lite} Zeiss; Carl Zeiss Meditec AG 07740 Jena 2008, Germany).

The segmented version of retinal vessel structure contains the vessel silhouettes automatically extracted from the fundus photographs. The binary skeletal structure of retinal vessel structure was obtained with one single pixel in width, but without any change in relative location and configuration of each element. This procedure was applied for all analyzed structures. All the skeletonised images were obtained with the ImageJ skeletonising algorithm[43].

Images of a normal and pathological state retinal vessel structure are shown in Figures 1, 2.

Multifractal and lacunarity analysis was performed in two cases: 1) on the segmented images (seg.); 2) on the skeletonized (skl.) version.

Multifractal analyses were computed applying the standard box-counting algorithm to the digitized data, using the ImageJ software 1.48g[43] together with the FracLac plug-in V 2.5[38].

The algorithm for multifractal analysis was applied with the following options: 1) grid positions: 10; 2) calculating of grid calibers: scaled series; 3) multifractal data processing: standard; 4) optimizing option: show optimal sample only; 5) sampling method: full scan. An optimal interval of box sizes was applied for the multifractal analysis: 10 pixels (the

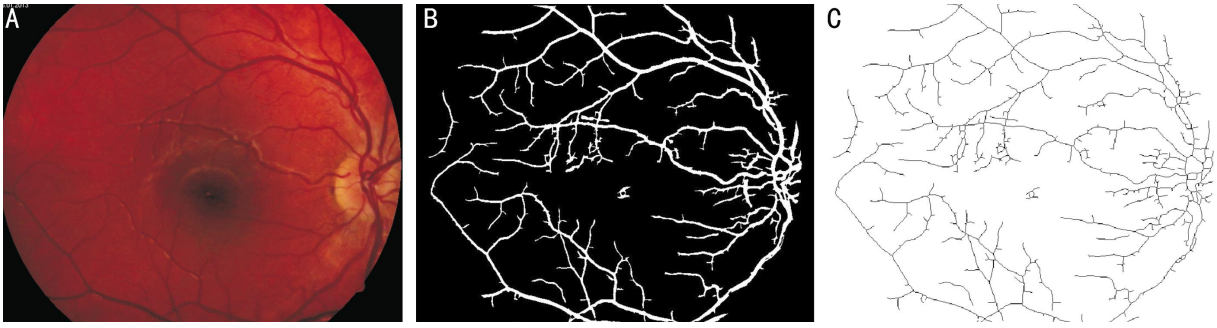

Figure 1 Image of a normal state retinal vessel network, right eye A: The color image version; B: The segmented version; C: The skeletonized version. The retinal vessels coming from the optic nerve have a normal branching pattern. The fundus has no sign of disease or pathology.

Figure 2 Image of an amblyopia state retinal vessel network, left eye A: The color image version; B: The segmented version; C: The skeletonized version. The retinal vessels coming from the optic nerve have a more complex branching pattern.

Table 1 The generalized dimensions (D_q) for q=0, 1, 2, and lacunarity parameter Λ with average±standard deviation, of 12 analyzed images, for normal and pathological status, in segmented and skeletonized variants

Status	Type	D_0	D_1	D_2	Λ
Normal (N)	Seg.	1.6926±0.0133	1.6266±0.0130	1.6016±0.0132	0.6766±0.1136
	Skl.	1.6689±0.0121	1.6249±0.0120	1.6002±0.0126	0.5820±0.0928
Pathological (P)	Seg.	1.7226±0.0131	1.6747±0.0134	1.6537±0.0132	0.5069±0.0659
	Skl.	1.6969±0.0123	1.6736±0.0126	1.6585±0.0125	0.4348±0.0319

D_0: The capacity (or box-counting) dimension; D_1: The information (Shannon entropy) dimension; D_2 : The correlation dimension. Statistically significant difference for all values, P<0.05.

minimum box size) and 60% from region of interest (the maximum box size).

Even if theoretically q should range from -∞ to +∞ to get a complete multifractal spectrum, the $f(\alpha)$ spectrum was computed in the range $-10 \leqslant q \leqslant 10$ for successive 0.25 steps (to show in detail the multifractal characteristic of the image), with special interest in values of q close to 0 and 2.

The algorithm for lacunarity analysis was applied using 5 to 20 pixel size boxes for each of four grid position on region of interest (ROI).

Statistical Analysis Microsoft Office Excel 2010 (Microsoft Corporation, Redmond, Washington, USA) statistical functions were used to determine (average ±standard deviation) of the generalized fractal dimensions (D_q) and lacunarity parameters Λ obtained with ImageJ software. All statistical calculations and analyses were done using GraphPad Instat (ver. 5.00, GraphPad Software) [44]. A Kruskal -Wallis non-parametric test for small samples was used. It was found that multifractal dimensions and lacunarity parameters Λ of the vascular trees followed a normal distribution. Differences with a P value of 0.05 or less were considered statistically significant. The average results were expressed as mean value and standard deviation.

RESULTS

Results of Multifractal and Lacunarity Analysis A summary of the obtained results is presented in the Table 1. The results for normal (N) status are: 1) in segmented variant: D_0=1.6926±0.0133; D_1=1.6266±0.0130; D_2=1.6016±0.0132; Λ=0.6766±0.1136; 2) in skeletonized variant: D_0=1.6689±0.0121; D_1=1.6249±0.0120; D_2=1.6002±0.0126; Λ=0.5820±0.0928. The results for pathological (P) status are: 1) in segmented variant: D_0=1.7226±0.0131; D_1=1.6747±0.0134; D_2=1.6537±0.0132; Λ=0.5069±0.0659; 2) in skeletonized variant: D_0=1.6969±0.0123; D_1=1.6736±0.0126; D_2=1.6585±0.0125; Λ=0.4348±0.0319.

The plots of geometrical representations obtained by multifractal analysis for normal retinal image (Figure 1B) and pathological retinal image (Figure 2B) analyzed with the ImageJ software are shown in Figures 3-6 and Figures 7-10, respectively.

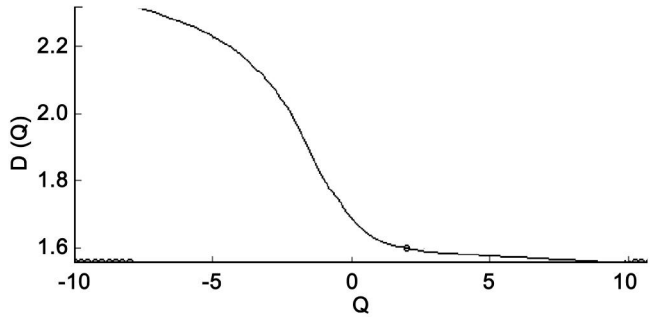

Figure 3 The $D(q)$ spectrum versus q for image (Figure 1B, segmented variant). D_0=1.6926; D_1=1.6266; D_2=1.6016.

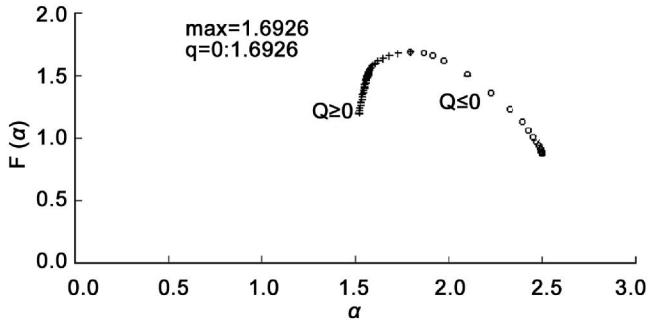

Figure 4 The $f(\alpha)$ spectrum versus α for image (Figure 1B, segmented variant). The left branch of the spectrum corresponds to large q values, while the right branch of the spectrum corresponds to small q values.

In Figure 3, the $D(q)$ curve versus q for image (Figure 1B, segmented variant) has a maximum value of 2.3179 in q = -7.75, then it has a decrease (from 2.3179 to 1.5586) for an increase of q (from -7.75 to 9.75). In Figure 4, the $f(\alpha)$ curve versus α for image (Figure 1B, segmented variant) has a maximum value of 1.6926 in α=1.7971 (corresponding to q =0). In Figure 5, the $f(\alpha)$ curve versus q for image (Figure 1B, segmented variant) rapidly increases (from q= -4.25 to q =0) to a maximum value of 1.6926 (for q =0), then slowly decreases and tends to 1.2 for q =9.5. In Figure 6, the $\alpha(q)$ curve versus q for image (Figure 1B, segmented variant) slowly decreases from 2.5027 (for q =-7.75) and tends to 1.5208 (for q=9.75).

In Figure 7, the $D(q)$ curve versus q for image (Figure 2B, segmented variant) has a maximum value of 2.4091 in q= -7.75, then it has a decrease (from 2.4091 to 1.5879) for an increase of q (from -7.75 to 9.5). In Figure 8, the $f(\alpha)$ curve versus α for image (Figure 2b, segmented variant) has a maximum value of 1.7226 in α =1.8096(corresponding to q=0). In Figure 9, the $f(\alpha)$ curve versus q for image (Figure 2B, segmented variant) rapidly increases (from q=-6.25 to q =0) to a maximum value of 1.7226 (for q =0), then linear decreases and tends to 1.1695 for q =9.5. In Figure 10, the $\alpha(q)$ curve versus q for image (Figure 2B, segmented variant) slowly decreases from 2.5783 (for q=-7.75) and tends to 1.5439 (for q=9.5).

Additionally, it can be noted that the multifractal spectra $D(q)$ and $f(\alpha)$ are interrelated and their shape provides

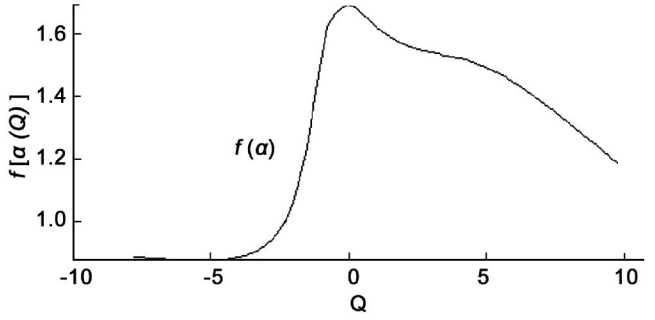

Figure 5 Plot of $f(\alpha)$ versus q for image (Figure 1B, segmented variant).

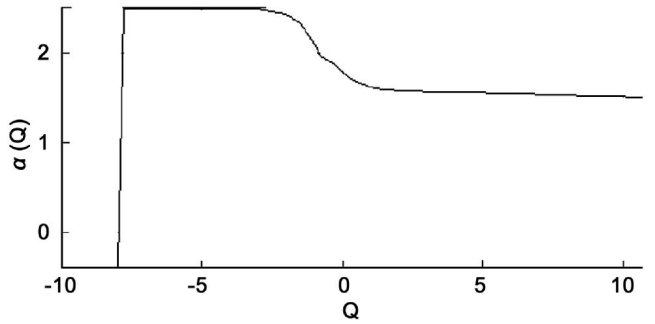

Figure 6 Plot of $\alpha(q)$ versus q for image (Figure 1B, segmented variant).

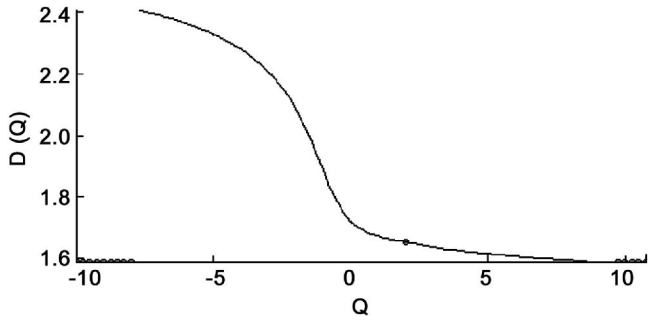

Figure 7 The $D(q)$ spectrum versus q for image (Figure 2B, segmented variant). D_0 =1.7226; D_1=1.6747; D_2=1.6537.

equivalent descriptions for retinal vascular network geometry, both characterizing the interwoven ensemble of fractal dimensions (Figures 4, 8).

DISCUSSION

The retinal diseases modify the human retinal microvascular network. The complex three-dimensional multifractal structure development of human retinal vessel arborisation is a nonuniform fractal which unlike a uniform fractal exhibits local density fluctuations and can be estimated using the multifractal geometry. The multifractal spectrum (associated with the geometrical features and spatial distribution of branching pattern of retinal vessel networks) describes the quality and quantity of irregularities in the data. On the other hand, the geometrical multifractality of the human retinal microvascular network is reflected in the non-uniformity of the distribution.

The (D_q) values for q=0, 1, 2, obtained for normal (N) and pathological (P) status, in segmented and skeletonized

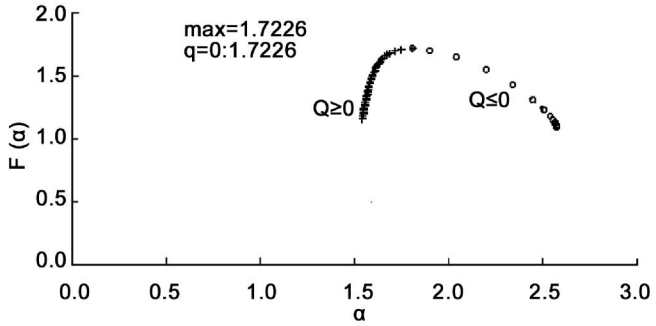

Figure 8 The $f(\alpha)$ spectrum versus α for image (Figure 2B, segmented variant). The left branch of the spectrum corresponds to large q values, while the right branch of the spectrum corresponds to small q values.

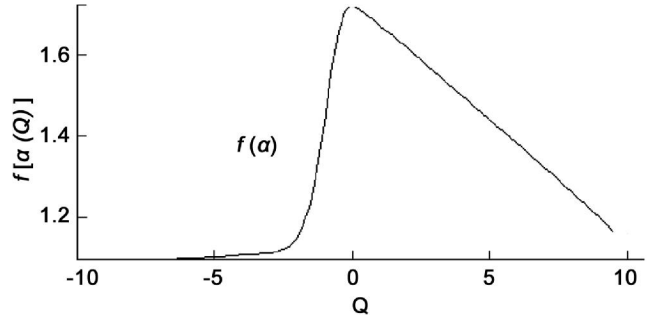

Figure 9 Plot of $f(\alpha)$ versus q for image (Figure 2B, segmented variant).

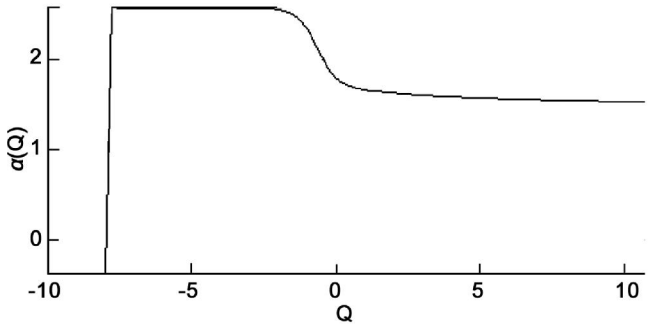

Figure 10 Plot of $\alpha(q)$ versus q for image (Figure 2B, segmented variant).

variants, are different and satisfy the inequality: $D_0 > D_1 > D_2$ where D_0 provides global (or average) information about the structure, D_1 quantifies the degree of disorder present in the distribution, and D_2 measures the mean distribution density of the statistical measure. The multifractal structure of the retinal microvascular network was validated by the statistically significant difference between D_0, D_1 and D_2. It can be noted, for normal (N) status, the values of generalized dimensions (D_q) for q =0, 1, 2 and the lacunarity parameter Λ are higher in segmented version than in skeletonized version. In pathological (P) status, the values of generalized dimensions (D_q) for q =0, 1 and the lacunarity parameter Λ are higher in segmented version than in skeletonized version.

The graphs (Figures 3, 7) revealed non-linear behaviour of the $D(q)$ spectrum versus q. The $f(\alpha)$ spectrum at the left and right of the maximum corresponds to $q>0$ and $q<0$, respectively. For α defined in [α_{min}, α_{max}], the curve $f(\alpha)$ is a smooth, single-humped, concave function, with $f(\alpha)>0$. For the graphs (Figures 4, 8) the maximum fractal dimension $f_{max}=D_0$ and the right shoulder of the curve $f(\alpha)$ is much longer than the left shoulder, that denotes an asymmetry of the $f(\alpha)$-α spectrum shape. It can also be noted that for q=1, the $f(\alpha)$ curve is tangent to the curve $f=\alpha$. The coefficients of correlation (R^2) of all linear fits were equal to or greater than 0.9925 representing a good linear correlation.

The quantitative measurement of the degree of multifractality is highlighted in the width of the $f(\alpha)$ curve (the difference $\Delta\alpha=\alpha_{max}-\alpha_{min}$) and in the range of the (D_q) values: for a larger $\Delta\alpha$ and a wider range, the non-uniformity of distribution is greater.

The deviation of the retinal microvascular network from translational or rotational invariance in digital retinal images was estimated using the lacunarity parameter Λ.

Multifractal analysis of the amblyopia images (segmented and skeletonized versions) show a higher average of the generalized dimensions (D_q) for q =0, 1, 2 indicating a higher degree of the tree-dimensional complexity associated with the human retinal microvasculature network whereas images of healthy subjects show a lower value of generalized dimensions indicating normal complexity of biostructure. On the other hand, the lacunarity analysis of the amblyopia images (segmented and skeletonized versions) show a lower average of the lacunarity parameter Λ than the corresponding values for normal images (segmented and skeletonized versions).

Taking into consideration the generalized dimensions (D_q) for q =0, 1, 2, and lacunarity parameter it can be noted that these ones may be markers of changes in retinal vascular architecture.

The simplicity and fast implementation, make the multifractal and lacunarity analysis of human retinal blood vessels a suitable tool for being integrated into a complete prescreening system for early diagnosis of patients with amblyopia. Theoretical understanding of the three-dimensional human retinal microvascular network, combined with the development of computational algorithms for computer-aided modelling and multifractal analysis allows new avenues to improve the investigations and clinical interpretations. The proposed methods may offer clear advantages and have the potential to complement the interpretation of the ophthalmologists and supply a computer-aided diagnosis system.

ACKNOWLEDGEMENTS

The authors would like to thank the participants and their families for participating in this study.

Conflicts of Interest: Tălu S, None; **Vlădutiu C,** None; **Lupaşcu CA,** None.

REFERENCES

1 Wright KW, Spiegel PH, Thompson LS (Eds.). *Handbook of pediatric strabismus and amblyopia*. USA:Springer Science+Business Media Inc.; 2006

2 Conner IP. *fMRI studies of amblyopia: pediatric and adult perspectives*. School of Medicine at West Virginia University, USA; 2005

3 McKee SP, Levi DM, Movshon JA. The pattern of visual deficits in amblyopia. *J Vis* 2003;3(5):380–405

4 Tălu SD. *Ophtalmologie–Cours*. Romania:Medical Publishing House "Iuliu Hatieganu"; 2005

5 Tălu S, Baltă F, Tălu SD, Merticariu A, Tălu M. Fourier domain–optical coherence tomography in diagnosing and monitoring of retinal diseases. *IFMBE Proceedings* 2009;26:261–266

6 Holz FG, Spaide RF (Eds). *Medical Retina. Focus on Retinal Imaging*. Germany: Springer–Verlag; 2010

7 Tălu S. Mathematical models of human retina. *Oftalmologia* 2011;55(3): 74–81

8 Tălu SD, Tălu S. Use of OCT imaging in the diagnosis and monitoring of age related macular degeneration. In Gui–Shuang Y, ed. *Age related macular degeneration–the recent advances in basic research and clinical care*. Croatia: InTech;2012;2(13):253–272

9 Tălu S, Giovanzana S. Fractal and multifractal analysis of human retinal vascular network: a review. *HVM Bioflux* 2011;3(3):205–212

10 Joshi VS. *Analysis of retinal vessel networks using quantitative descriptors of vascular morphology*. University of Iowa; 2012

11 Tălu S. Characterization of retinal vessel networks in human retinal imagery using quantitative descriptors. *HVM Bioflux* 2013;5(2):52–57

12 Tălu S. Multifractal geometry in analysis and processing of digital retinal photographs for early diagnosis of human diabetic macular edema. *Curr Eye Res* 2013;38(7):781–792

13 Heringa SM, Bouvy WH, van den Berg E, Moll AC, Kappelle LJ, Biessels GJ. Associations between retinal microvascular changes and dementia, cognitive functioning, and brain imaging abnormalities: a systematic review. *J Cereb Blood Flow Metab* 2013;33(7):983–995

14 Cheung CY, Lamoureux E, Ikram MK, Sasongko MB, Ding J, Zheng Y, Mitchell P, Wang JJ, Wong TY. Retinal vascular geometry in Asian persons with diabetes and retinopathy. *J Diabetes Sci Technol* 2012;6(3):595–605

15 Lim LS, Cheung CY, Sabanayagam C, Lim SC, Tai ES, Huang L, Wong TY. Structural changes in the retinal microvasculature and renal function. *Invest Ophthalmol Vis Sci* 2013;54(4):2970–2976

16 Gopinath B, Chiha J, Plant AJ, Thiagalingam A, Burlutsky G, Kovoor P, Liew G, Mitchell P. Associations between retinal microvascular structure and the severity and extent of coronary artery disease. *Atherosclerosis* 2014;26;236(1):25–30

17 Losa GA, Merlini D, Nonnenmacher TF, Weibel E (Eds.). *Fractals in biology and medicine. Vol. IV*. Switzerland:Birkhäuser Verlag; 2005

18 Tălu S. Fractal analysis of normal retinal vascular network. *Oftalmologia* 2011;55(4):11–16

19 Tălu S, Giovanzana S. Image analysis of the normal human retinal vasculature using fractal geometry. *HVM Bioflux* 2012;4(1):14–18

20 Azemin MZ, Kumar DK, Wong TY, Wang JJ, Mitchell P, Kawasaki R, Wu H. Age–related rarefaction in the fractal dimension of retinal vessel. *Neurobiol Aging* 2012;33(1):194.e1–4

21 Tălu S. The influence of the retinal blood vessels segmentation algorithm on the monofractal. *Oftalmologia* 2012;56(3):73–83

22 Tălu S, Vlăduţiu C, Popescu LA, Lupaşcu CA, Vesa SC, Tălu SD. Fractal and lacunarity analysis of human retinal vessel arborisation in normal and amblyopic eyes. *HVM Bioflux* 2013;5(2):45–51

23 Patton N, Aslam TM, MacGillivray T, Deary IJ, Dhillon B, Eikelboom RH, Yogesan K, Constable IJ. Retinal image analysis: concepts, applications and potential. *Prog Retin Eye Res* 2006;25(1):99–127

24 Liberek I, Chaberek S, Anielska E, Kowalska K, Ostrowski K. Symmetry of retinal vessel arborisation in normal and amblyopic eyes. *Ophthalmologica* 2010;224(2):96–102

25 Olujic M, Miloševic NT, Oros A, Jelinek HF. *Aggressive posterior retinopathy of prematurity: fractal analysis of images before and after laser surgery*. In Dumitrache I, Ed. Romania: Politehnica Press; 2011;2:877–881

26 Tălu S, Fazekas Z, Tălu M, Giovanzana S. *Analysis of human peripapillary atrophy using computerised image analysis*. In: The 9th Conference of the Hungarian Association for Image Processing and Pattern Recognition (KEPAF 2013), January 29–February1, 2013, Bakonybél, Hungary:427–438

27 Tălu S. Multifractal characterization of human retinal blood vessels. *Oftalmologia* 2012;56(2):63–71

28 Stosic T, Stosic B. Multifractal analysis of human retinal vessels. *IEEE Trans Med Imaging* 2006;25(8):1101–1107

29 Tălu S. Mathematical methods used in monofractal and multifractal analysis for the processing of biological and medical data and images. *ABAH Bioflux* 2012;4(1):1–4

30 Tălu S. Texture analysis methods for the characterisation of biological and medical images. *ELBA Bioflux* 2012;4(1):8–12

31 Fraz MM, Remagnino P, Hoppe A, Uyyanonvara B, Rudnicka AR, Owen CG, Barman SA. Blood vessel segmentation methodologies in retinal images–a survey. *Comput Methods Programs Biomed* 2012;108(1):407–433

32 Tălu S, Tălu M. *Influence of image processing on the measurement of the human retinal microvascular fractal dimension*. In: International Conference of Mechanical Engineering (ICOME 2013), May 16–17, 2013, Craiova, Romania, Proceedings, Tome 1, Universitaria Publishing House Craiova:105–112

33 Chhabra A, Jensen RV. Direct determination of the f (α) singularity spectrum. *Phys Rev Lett* 1989;62:1327–1330

34 Stach S, Cybo J. Multifractal description of fracture morphology: theoretical basis. *Mater Charact* (2003);51(1):79–86

35 Hu MG, Wang JF, Ge Y. Super–resolution reconstruction of remote sensing images using multifractal analysis. *Sensors* 2009;9(11):8669–8683

36 Shi K, Liu CQ, Ai NS. Monofractal and multifractal approaches in investigating temporal variation of air pollution indexes. *Fractals* 2009;17 (4):513–521

37 Plotnick RE, Gardner RH, Hargrove WW, Prestegaard K, Perlmutter M. Lacunarity analysis: a general technique for the analysis of spatial patterns. *Physical Review E* 1996;53(5):5461–5468

38 FracLac V 2.5 for ImageJ software (A. Karperien–Charles Sturt University, Australia). Available from: http://rsbweb.nih.gov/ij/plugins/fraclac/FLHelp/Introduction.htm. 1999–2013. Accessed July 30, 2015

39 Dobrescu R, Ichim L, Crişan D. Diagnosis of breast cancer from mammograms by using fractal measures. *International Journal of Medical Imaging* 2013;1(2):32–38

40 Lupaşcu CA, Tegolo D, Trucco E. A comparative study on feature selection for retinal vessel segmentation using FABC. In Proc. of CAIP 2009, Germany;2009:655–662, Lecture Notes in Computer Science (LNCS) 5702, Berlin Heidelberg; Springer–Verlag;2009

41 Lupaşcu CA, Tegolo D, Trucco E. FABC: Retinal vessel segmentation using AdaBoost. *IEEE Trans Inf Technol Biomed* 2010;14(5):1267–1274

42 Lupaşcu CA, Tegolo D. *Stable automatic unsupervised segmentation of retinal vessels using Self–Organizing Maps and a modified Fuzzy C–Means clustering*. Proc. of WILF 2011, Italy;2011:244–252, Lecture Notes in Artificial Intelligence (LNAI 6857), Subseries of Lecture Notes in Computer Science (LNCS), Berlin Heidelberg;Springer–Verlag; 2011

43 ImageJ software, version ImageJ 1.48g (Wayne Rasband, National Institutes of Health, Bethesda, Maryland, USA). Available from: http://imagej.nih.gov/ij. Accessed July 30, 2015

44 GraphPad InStat software, version 5.00 (GraphPad, San Diego, California, USA). Available from: http://www.graphpad.com/instat/instat.htm. Accessed July 30, 2015